Multipactor Breakdown Analysis of Ku-Band Meandered Low-Pass Filter

A. Sami[(1)], F. Teberio[(1)], I. Arnedo[(1)], P. Martin-Iglesias[(1)-(2)], T. Lopetegi[(1)], M. A. G. Laso[(1)], and I. Arregui[(1)]

[(1)] Institute of Smart Cities (ISC), Department of Electrical, Electronic, and Communication Engineering, Public University of Navarre (UPNA), 31006 Pamplona, Spain
abdul.sami@unavarra.es, fernando.teberio@unavarra.es, israel.arnedo@unavarra.es, txema.lopetegi@unavarra.es, mangel.gomez@unavarra.es, ivan.arregui@unavarra.es.

[(2)] European Space Agency (ESA)-ESTEC, 2201 Noordwijk, The Netherland
Petronilo.martin.iglesias@esa.int

INTRODUCTION

The multipactor discharge is one of those phenomena in passive components which can potentially cause the loss of the satellite signals or their distortion. Furthermore, in the extreme case, it can damage the components or even the subsystems due to the excessive reflected power [1]-[2]. The electrons get accelerated in vacuum under a strong electric field. These accelerated electrons can release secondary electrons when they strike a surface with enough energy. The secondary electrons in return get synchronized with the electric field inside the component and are accelerated to strike the component surface to release further electrons. If the multiplication of an ample number of electrons sustains, the number of the electrons inside the component grows exponentially, which leads to the multipactor breakdown at high input powers. Therefore, passive components with high power handling capabilities are required to prevent multipactor discharge. Nowadays, high power satellites up to 20 kW are being developed to increase the capacity, especially in the telecommunication sector. Depending on the system architecture, the antenna feed system for these satellites can be made of different components such as magic-tees, waveguide bends, diplexers, etc. Filters are considered to be the most fragile element when it comes to high power handling capability because of their resonant nature. This becomes crucial when a single antenna is used for both reception and transmission, where the two different frequency bands are separated by diplexers and hence more power can go through the antenna feed. which requires high-power handling filters and diplexers to avoid multipactor discharge [3].

Many design techniques have been reported in the past to develop high-power low-pass filter (LPF) [4]. For instance, in [5]-[6], E-plane low-pass high-power corrugated filters with wide rejection bands have been presented using in-line topologies for Ku-band applications. Novel topologies with flexible routing capabilities were implemented using stepped-impedance structures based on commensurate lines in [7]-[8] to design band-pass filters with a reduced footprint. The design technique presented in [8] has also been employed to design meander-shaped LPF with large mechanical gaps.

In this work, a very compact rectangular waveguide low-pass filter with meandered topology based on commensurate lines for Ku-band satellite applications is analysed for high-power handling capabilities. The device consists of rectangular waveguide sections properly cascaded to form a meandered topology to obtain the desired value of the local reflection coefficients. which are essential to achieve the target frequency response and also to keep large mechanical gaps. Hence, this technique allows us not only to design a filter with compact size but a filter geometry which is suitable for high power applications. In the paper, the low-pass filter based on commensurate lines is first designed by cascading E-plane mitered bends ($\pm 90°$ EMBs) in CST Microwave Studio (MWS) and then the values of the electromagnetic fields at the passband frequencies are exported to Spark3D to perform a multipactor analysis. The critical areas inside the device where the multipactor discharge occurs will also be identified in the high-power analysis.

DESIGN METHODOLOGY OF MEANDERED LPF

The design process of the meandered LPF starts by fixing the order n of the filter for the given frequency response, f_c, the cut-off frequency of the passband, f_0, the stopband frequency with the largest attenuation, R_L, the in-band return-loss level, and the type of all-pole filtering function employed (for instance, Chebyshev). The guided wavelength $\lambda_{g(f_c)}$ and $\lambda_{g(f_0)}$ which correspond to f_c and f_0 respectively, are related to the electrical length θ_c as given in [8]:

$$\theta_c = \frac{\pi}{2} \cdot \frac{\lambda_{g(f_0)}}{\lambda_{g(f_c)}} \tag{1}$$

As the LPF is based on commensurate lines with stepped-impedance geometry, it is necessary to calculate the characteristic impedances Z_n of the stepped-impedance sections for the given all-pole filter function. The value of the characteristics impedance of each waveguide section can be calculated by applying the Richard's transformation explained in [9]. Then the local reflection coefficient Γ_n which appears due to the mismatch at the junction between the stepped-impedance sections can be calculated as given in [8]:

$$\Gamma_n = \frac{Z_n - Z_{n-1}}{Z_n + Z_{n-1}} \tag{2}$$

In order to implement the characteristic impedances using the meandered topology that will provide routing capability to the filter, a modular design strategy is followed where $\pm 90°$ EMBs (see Fig. 1) with constant width a and varying heights b_{n-1}, b_n, b_{n+1} will be designed independently and then the $n+1$ EMBs will be cascaded together to realize the LPF. The sign of the $\pm 90°$ EMB is used to depict the orientation of the EMB, as can be seen in Fig. 2. The reflection coefficient Γ_n is directly related to the contrast between b_{n-1} and b_n of the *n*th-EMB. As the value of b_0 is fixed depending upon the desired minimum mechanical gap, which is key to achieve a high-power handling capability and also the stopband performance, the next step is to calculate the rest of the heights in iterative manner by fulfilling the condition $|S_{11,n}(f_c)| = |\Gamma_n|$, where for $b_{n-1} < b_n$ then $\Gamma_n > 0$, and for $b_{n-1} > b_n$ then $\Gamma_n < 0$. Although Γ_n is mainly dependent on the contrast between b_{n-1} and b_n , the effect of the tilt of the chamfer at the input $t_{n,ip}$ and output $t_{n,op}$ must be considered in the design process. The tilt of the chamfer is useful in order to avoid extreme height excursions. Then, the lengths $(l_{n,ip}, l_{n,op})$ must be calculated considering the phase conditions given in [8] for the type of step ($b_{n-1} < b_n, b_{n-1} > b_n$). Finally, the l_n are calculated following: $l_n = l_{i,op} + l_{i+1,ip}$, since the output of the *n*th-EMB and the input of the *n*+1th-EMB share the same height [8]. Apart from achieving the largest minimum mechanical gaps, meandered topology can be employed to create transmission zeros in the stopband. The transmission zeros are created due to the interference of the TE_{10} mode with higher modes that are excited due to bends [8]. Once all the EMBs are designed for a given frequency behaviour, the next step is to assemble them together to form a complete filter (as shown in Fig. 3). The sequence of the '+' and '−' EMBs defines the geometry of the filter.

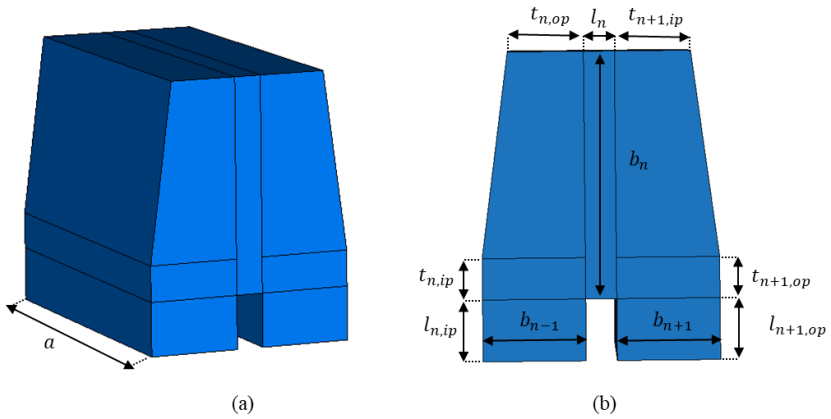

Fig. 1. Schematic of the nth ±EMB. (a) 3D schematic, (b) Side view.

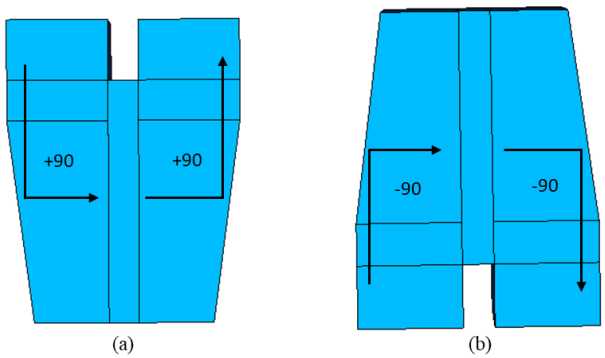

Fig. 2. (a) Orientation of the +EMB, (b) Orientation of the −EMB.

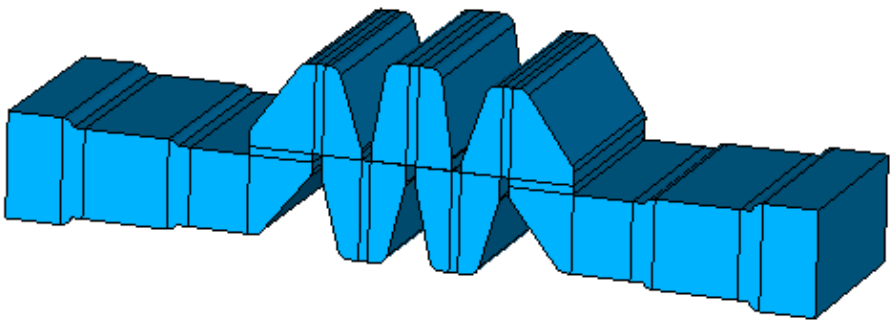

Fig. 3. 3D schematic of the high-power LPF with meandered topology.

MULTIPACTOR ANALYSIS

A LPF must be designed before performing its multipactor analysis following the design method discussed above. In this paper, a 11th-order Chebyshev filter has been designed with in-band return loss equal to 25 dB between 10.7 and 11.7 GHz, $f_c = 11.85$ GHz and $f_0 = 17$ GHz. The filter width is fixed to $a = 19.05$ mm and the height of the input cavity is $b_0 = 7$ mm. The Richard's transformation has been applied to extract the normalized characteristics impedances ($Z_0 = Z_{12} = 1.0, Z_1 = Z_{11} = 0.75, Z_2 = Z_{10} = 1.32, Z_3 = Z_9 = 0.60, Z_4 = Z_8 = 1.62, Z_5 = Z_7 = 0.53, Z_6 = 1.69$) for the aforementioned specifications. Then, using (2), the values of the local reflection coefficients, Γ_n, are calculated. Once the values of the Γ_n are obtained, the next step is to compute the dimensions of the nth $\pm 90°$ EMB ($t_{n,ip}$, $t_{n,op}$ and b_n) following the condition $|S_{11,n}(f_c)| = \Gamma_n$ while bearing in mind that the value of the $b_0 = 7$ mm has been already fixed. The values of the $l_{n,ip}$ and $l_{n,op}$ are computed satisfying the phase conditions explained in [8]. All the dimensions are listed in Table 1. The sequence of EMBs to implement meandered topology is: $+--++--\cdots+$, which produces three transmission zeros near the passband. Furthermore, the topology helped us to obtain a minimum mechanical gap equal to 3.224 mm which will enhance the high-power handling capability of the device. The schematic of the filter is shown in Fig. 3 while the simulated frequency response is shown in Fig. 4.

Table 1. Dimensions of the meandered LPF (mm).

Parameter	Value	Parameter	Value	Parameter	Value	Parameter	Value
$b_0 = b_{12}$	7.0	$l_0 = l_{12}$	5.0	$t_{1,ip} = t_{12,op}$	1.0	$t_{1,op} = t_{12,ip}$	1.00
$b_1 = b_{11}$	5.77	$l_1 = l_{11}$	1.00	$t_{2,ip} = t_{11,op}$	1.16	$t_{2,op} = t_{11,ip}$	1.50
$b_2 = b_{10}$	7.96	$l_2 = l_{10}$	0.86	$t_{3,ip} = t_{10,op}$	0.81	$t_{3,op} = t_{10,ip}$	1.23
$b_3 = b_9$	3.56	$l_3 = l_9$	0.05	$t_{4,ip} = t_{9,op}$	1.68	$t_{4,op} = t_{9,ip}$	2.00
$b_4 = b_8$	8.95	$l_4 = l_8$	1.10	$t_{5,ip} = t_{8,op}$	1.65	$t_{5,op} = t_{8,ip}$	1.56
$b_5 = b_7$	3.22	$l_5 = l_7$	0.05	$t_{6,ip} = t_{7,op}$	1.95	$t_{6,op} = t_{7,ip}$	1.07
b_6	8.84	l_6	0.61	-	-	-	-

The multipactor analysis can be performed in SPARK3D once the LPF is designed and simulated in CST Microwave Studio (MWS). The electromagnetic fields are simulated at 10.70, 10.95, 11.2, 11.45, and 11.7 GHz, and exported to SPARK3D to perform the multipactor analysis as the operating frequency range of the filter is between 10.7 and 11.7 GHz. Silver (ECSS) is used as the material in SPARK3D to estimate the input multipactor breakdown power. The initial power value is set to 5kW with an initial number of electrons equal to 5000. First, the multipactor analysis was performed by considering the whole circuit, and then the multipactor analysis was performed considering only specific small regions in order to identify the critical areas in the circuit. The multipactor analysis at 10.70 and 10.95 GHz is presented in Fig. 5 and 7, where the estimated breakdown power values are 178 kW and 188 kW, respectively. Initially, the analysis was performed in the entire circuit, where the electrons inside the circuit are illustrated in Fig. 6 and 8 at 10.7 and 10.95 GHz. After that, the analysis was performed in smaller areas to identify the breakdown regions. The multipactor discharge was only observed at the input port (see left side of Fig. 6 and 8) at 10.70 and 10.95 GHz, while no breakdown was observed inside the filter structure. At 11.2 GHz, the breakdown happens at the input port similar to the previous frequencies at input power equals to 189 kW. Similarly, the multipactor analysis was performed at 11.45 GHz as shown in Fig. 9. The multipactor breakdown happens at 42.74 kW and the breakdown occurs at two different areas around the central part of the structure, as indicated in Fig. 10. Finally, the multipactor analysis was performed at 11.7 GHz which is near to the upper passband edge where the electric fields have maximum values. The multipactor analysis at 11.7 GHz is shown in Fig. 11, where the estimated input breakdown power is 20.8 kW, which is the minimum threshold power of the device. The most important part of the analysis is to compute the minimum input breakdown power and also the corresponding breakdown area. The critical area at 11.7 GHz is shown in Fig. 12, which also coincides with the minimum mechanical gap ($b_5 = b_7$= 3.224 mm) of the structure. Hence, the minimum gap located around the central part of the structure is the parameter which determines the minimum input threshold power of the device. Therefore, the minimum input threshold power can be increased by increasing the minimum gap if desired. In this case, the device has a meandered topology that is implemented with the help of chamfers in the cavities. The tilt of the chamfer ($t_{n,ip}$ and $t_{n,op}$) gives us an extra degree of freedom to implement the required value of Γ_n along with the height (b_{n-1}, b_n, b_{n+1}). In consequence, the minimum gap can be increased by increasing the value of the tilt to the optimum level in order to further increase the minimum input threshold power.

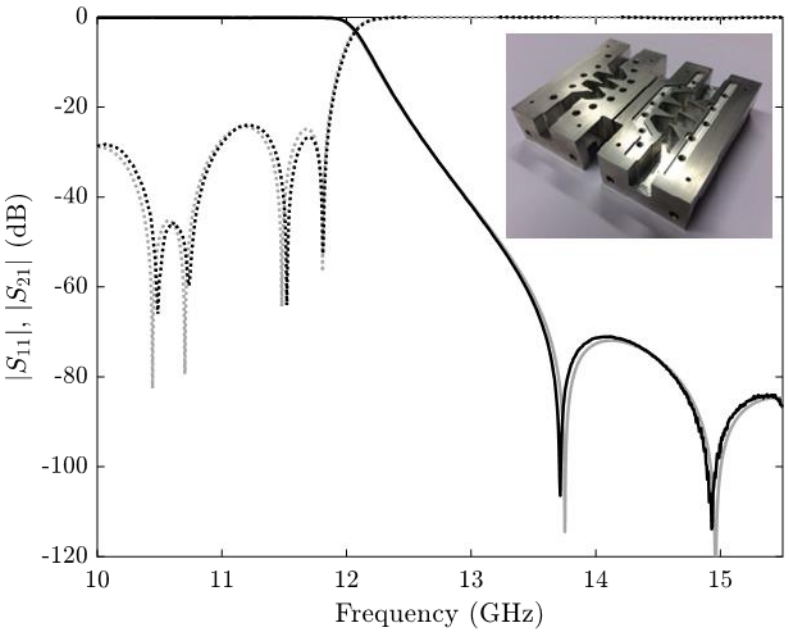

Fig. 4. Frequency response of the high-power LPF. The simulated results are given with gray lines and measured results are given with black lines. $|S_{11}|$ in dotted line, $|S_{21}|$ in solid line. Inset: photograph of the unassembled prototype.

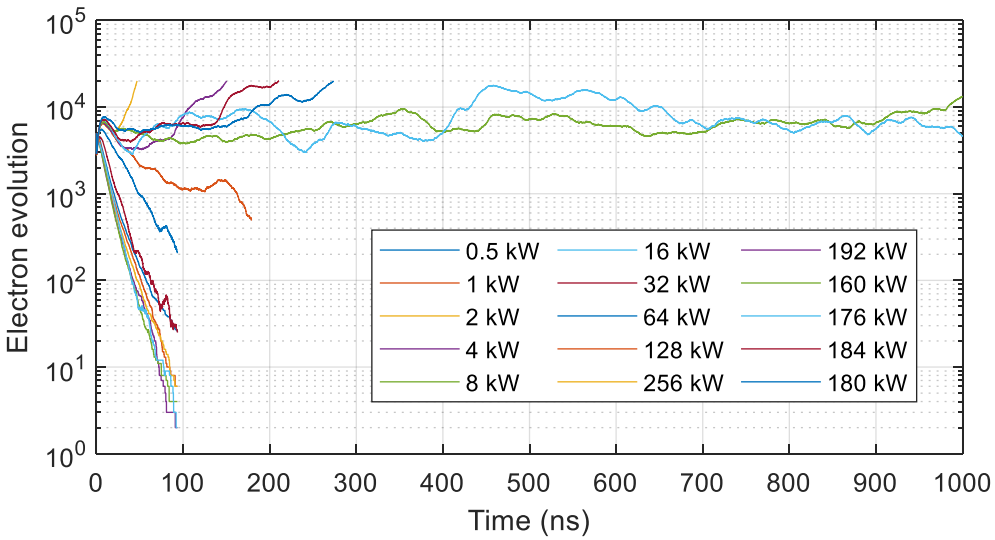

Fig. 5. Multipactor analysis at 10.7 GHz: the input breakdown power value is 178 kW.

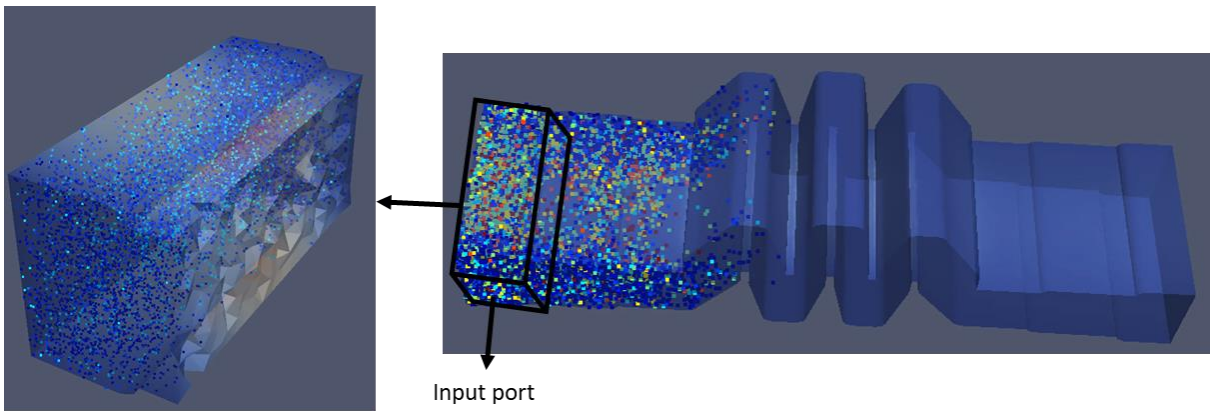

Fig. 6. Illustration of multipactor breakdown inside the circuit at 10.7 GHz.

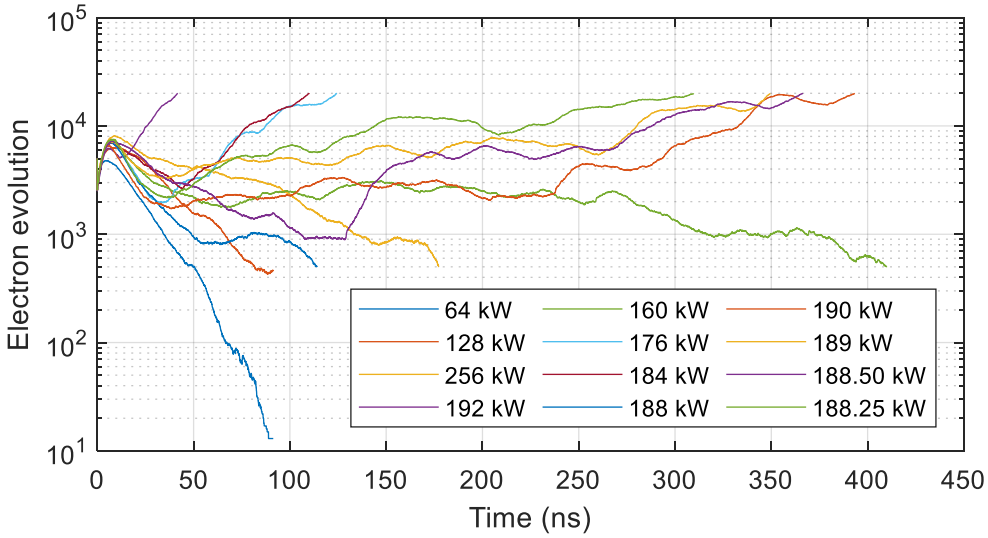

Fig. 7. Multipactor analysis at 10.95 GHz: the input breakdown power value is 188 kW.

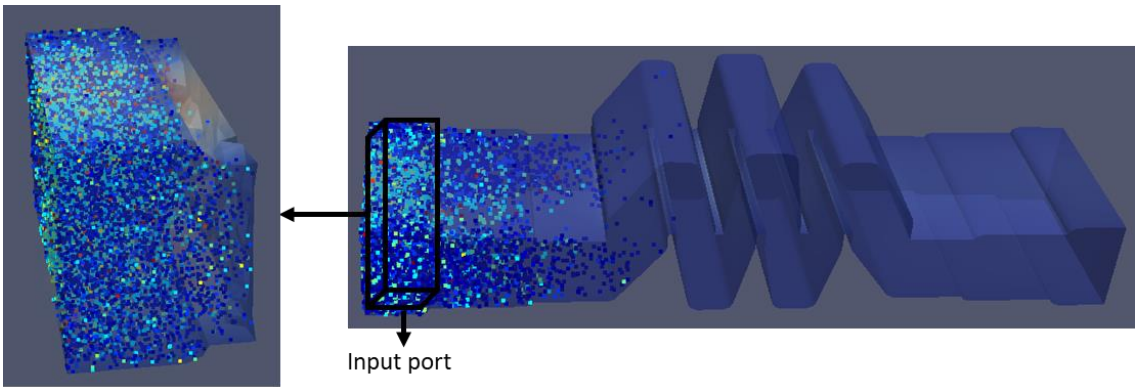

Fig. 8. Illustration of multipactor breakdown inside the circuit at 10.95 GHz.

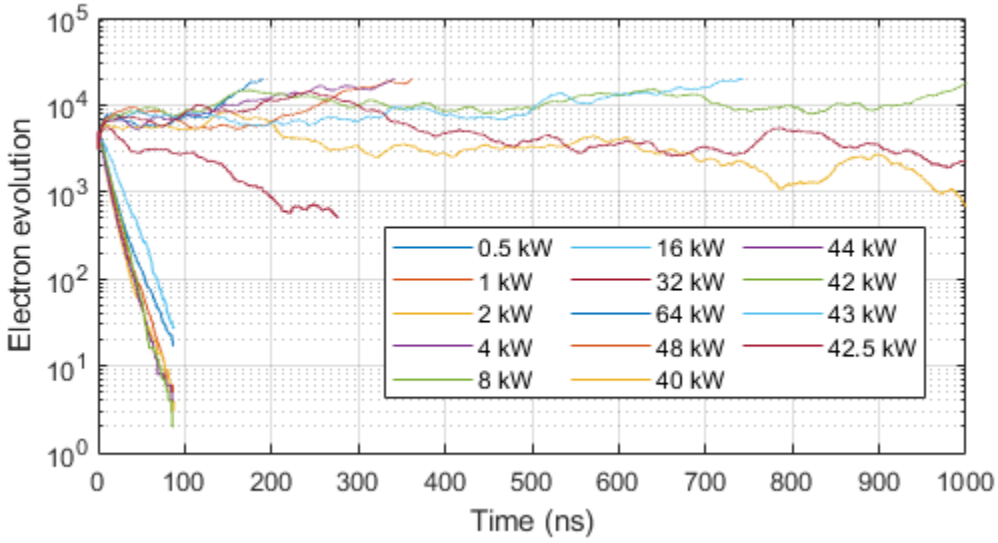

Fig. 9. Multipactor analysis at 11.45 GHz: the input breakdown power value is 42.74 kW.

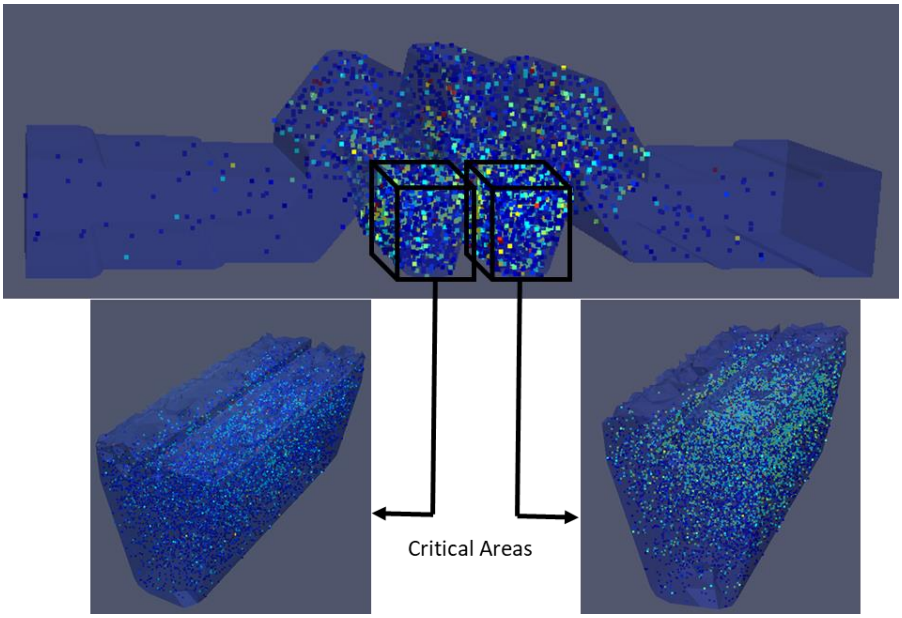

Fig. 10. Illustration of multipactor breakdown inside the circuit at 11.45 GHz.

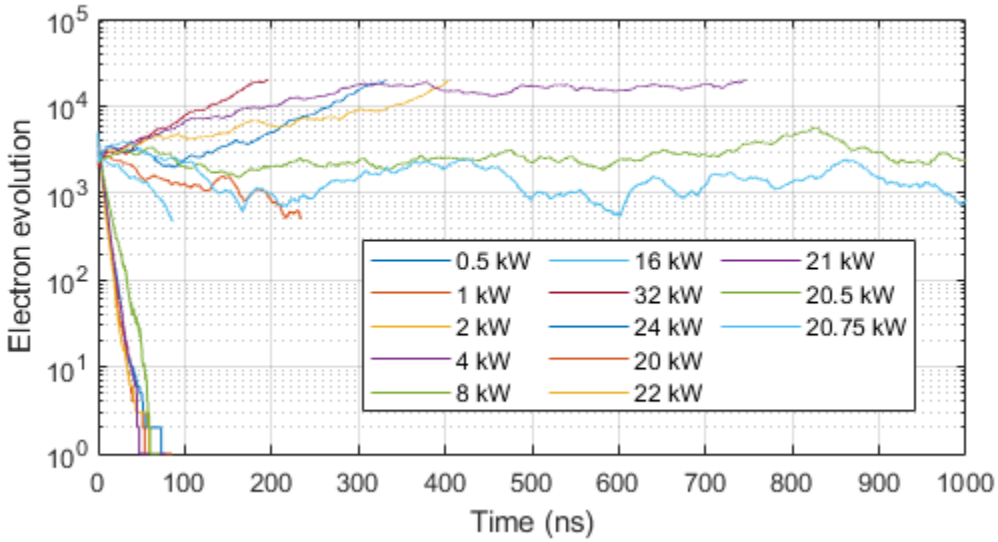

Fig. 11. Multipactor analysis at 11.7 GHz: the input breakdown power value is 20.8 kW.

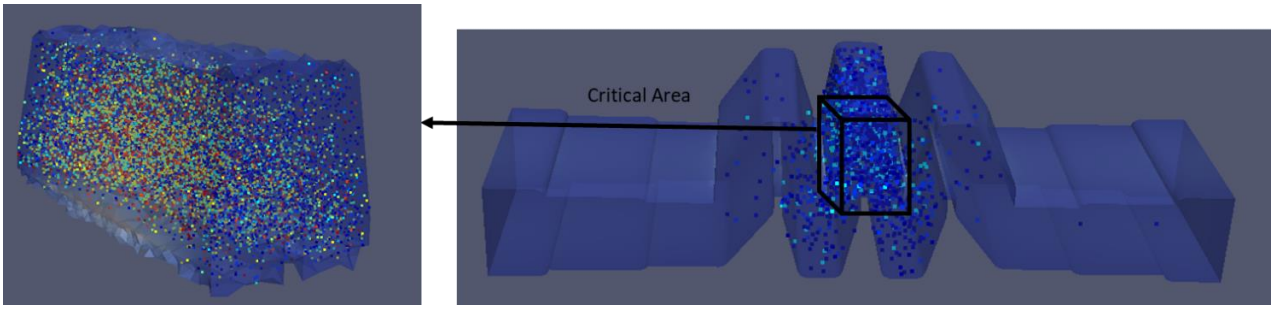

Fig. 12. Illustration of multipactor breakdown inside the circuit at 11.7 GHz.

CONCLUSION

A low-pass high-power meander-shaped filter is designed with high-power handing capabilities for Ku-band satellite applications. The meandered topology is obtained by cascading $\pm 90°$ EMBs aiming to achieve larger minimum mechanical

gaps that increase the multipactor threshold at the operating frequency range between 10.7-11.7 GHz. The high-power behaviour of the device is illustrated through a multipactor analysis using SPARK3D at 10.7, 10.95, 11.2, 11.45 and 11.7 GHz, where the critical circuit areas are also identified. The breakdown occurs at different areas at different frequencies and the minimum estimated input threshold power is computed to be 20.8 kW at 11.7 GHz in a region of minimum mechanical gap. The multipactor analysis helps to identify the key design parameters that can be exploited to further enhance the power handling capability of the device.

ACKNOWLEDGMENTS

This work was supported by the Spanish Ministerio de Ciencia e Innovación –Agencia Estatal de Investigación (MCIN/AEI/ 10.13039/501100011033) under Project PID2020-112545RB-C53 and by the European Union's Horizon 2020 Research and Innovation Program under Grant 811232-TESLA-H2020-MSCA-ITN-2018.

REFERENCES

[1] V.E. Semenov, et al., "Conformal mapping analysis of multipactor breakdown in waveguide irises", *Physics of Plasmas*, vol. 15, no. 3, 2008.

[2] N. Balcon, D. Payan, M. Belhaj, T. Tondu and V. Inguimbert, "Secondary electron emission on space materials: Evaluation of the total secondary electron yield from surface potential measurements", *IEEE Transactions on Plasma Science*, vol. 40, no. 2, pp. 282-290, 2011.

[3] P. Sarasa, et al., "Comparative study of the power handling capability of space broadband antenna filters in Ku-band", *Proc. 5th int. Workshop Multipactor, Corona Passive Intermodulation Space RF Hardware. (MULCOPIM)*, 2005.

[4] I. Arregui, et al, "High-power filter design in waveguide technology: future generation of waveguide satellite filters in payloads handling increasing bit rates and numbers of channels", in *IEEE Microwave Magazine*, vol. 21, no. 6, pp. 46-57, 2020.

[5] I. Arregui, et al., "Multipactor prediction in novel high-power low-pass filters with wide rejection band," *European Microwave Conference (EuMC), IEEE*, 2009.

[6] I. Arregui, et al., "Multipactor-resistant low-pass harmonic filters with wide-band higher-order mode suppression", *IEEE MTT-S International Microwave Symposium Digest*, 2013.

[7] A. Sami, et al., "Robust tolerance design of bandpass filter with improved frequency response for Q-band satellite applications", *Microwave and Wireless Components Letters*, vol. 31, no. 11, pp. 1183-1185, November 2021.

[8] F. Teberio, et al., "Rectangular waveguide filters with meandered topology", *IEEE Transactions on Microwave Theory and Techniques*, vol. 66, no. 8, August 2018.

[9] R. J. Cameron, C. M. Kudsia and R. R. Mansour, *"Microwave filters for communication systems: fundamentals, design and applications"*, Hoboken, NJ, USA: Wiley, 2007.